Available online at www.sciencedirect.com
ScienceDirect
Optical Materials 29 (2007) 623–630
OPTICAL Materials
www.elsevier.com/locate/optmat

Wavelength dependence of the photo-electromotive-force effect in CdTe:V crystal with bipolar photoconductivity

S. Stepanov [a,*], P. Rodríguez [b], S. Mansurova [b], M.L. Arroyo [c], S. Trivedi [d], C.C. Wang [d]

[a] CICESE, 107 km, Carretera Tijuana-Ensenada, Ensenada, B.C. 22860, Mexico
[b] INAOE, Apartado Postal 51 y 216, Puebla, Pue. 72000, Mexico
[c] BUAP, Apartado Postal 1152, Puebla, Pue. 72000, Mexico
[d] Brimrose Corp. of America, 7720 Belair Road, Baltimore, MD 21236, USA

Received 8 July 2005; accepted 22 October 2005
Available online 10 January 2006

Abstract

We report on detailed investigation of the photo-electromotive-force (photo-EMF) effect in semiconductor with bipolar photoconductivity of impurity type in a spectral region close to the fundamental absorption edge, where both the photoconductivity and the photo-EMF response reach their maxima. The experiments performed with CdTe:V crystal ($\Delta E \approx 1.51$ eV) in the spectral range of 826–853 nm show that dynamics of the photo-EMF signal formation in this crystal is governed by relaxation of slow majority photocarriers–holes with the life-time which goes down from $\tau \approx 9$ μs at 850 nm to ≈6.5 μs at 826 nm. The minority photocarriers (electrons), which contribute approximately 10% of the total photoconductivity, also demonstrate significant wavelength dependence of their diffusion length with $L_D \approx 8.5$ μm at 850 nm and ≈6.3 μm at 830 nm. The reported results show significant improvement in responsivity of the bipolar CdTe:V photo-EMF detector when it is operated at $\lambda = 840$ nm (by factor ≈2.5 as compared with that at 852 nm).

1. Introduction

The adaptive photodetectors based on the non-steady-state photo-electromotive force (photo-EMF) effect [1] attract attention due to possibility of deploying them for an adaptive interferometric detection of laser-induced ultrasonic waves (see Fig. 1) in industrial environment [2]. The photo-EMF effect in question is observed under illumination of a short-circuited photoconductive sample by the vibrating interference pattern. The appearing periodic (transient) photo-EMF current results from interaction of the vibrating pattern of photoconductivity with more inertial spatial distribution of the space charge electric field, which is formed via diffusion of the photoinduced carriers from maxima of the same illuminating interference pattern. The photo-EMF detectors are simple, robust, and demonstrate sufficiently high ($\geqslant$10–100 kHz) cut-off frequency. This enables their application to real-world objects with as-processed surfaces that can also be moving with velocities up to several m/s [3]. The main drawback, which impedes wide-spread adoption of these devices in practice, is insufficient sensitivity stemming from difficulties with matching of the high-impedance detector with the high-frequency transimpedance amplifier (which typically has the input noise current ~1 pA/Hz$^{1/2}$ [4]).

In the majority of publications on these applications (see, e.g. review papers [1,2]) detectors based on semiinsulating GaAs crystals and probe lasers with the wavelengths ranging from visible (532 nm) to near IR (820–850 nm) spectral regions are generally used. Selection of theses wavelengths is dictated by commercial availability of reliable, cost-effective cw laser sources (diode pumped frequency-doubled Nd:YAG solid state lasers and semiconductor GaAlAs lasers, respectively). It was shown in reference [5] that formation of the photo-EMF signal in semiinsulating GaAs crystal is governed by essentially

* Corresponding author. Tel.: +52 6461 750595; fax: +52 6461 750553.
E-mail address: steps@cicese.mx (S. Stepanov).

0925-3467/$ - see front matter © 2005 Elsevier B.V. All rights reserved.
doi:10.1016/j.optmat.2005.10.011

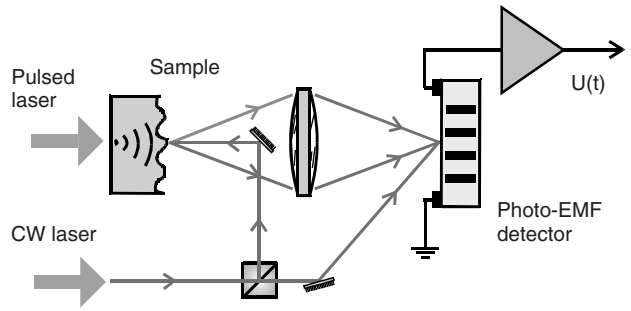

Fig. 1. Simplified configuration for adaptive detection of laser-induced ultrasound by means of photo-EMF detector.

bipolar photoconductivity of these semiconductors in visible–near IR spectral range. Recently, effective application of monopolar CdTe:V photo-EMF detectors for the above-mentioned near IR spectral region was also reported by our group [6–9]. Generally speaking, the monopolar photo-EMF detectors seem to be superior to the bipolar devices: due to electron–hole competition in the space charge grating formation, the bipolar photo-EMF detectors always have lower responsivity [1,5].

Utilization of asymmetric interdigitated contacts (AIDC's) [10,11] reduces the impedance of the photo-EMF device significantly and can be considered as an efficient solution for the detector/preamplifier matching problem. The detailed analysis published by our group recently [12] showed that for the range of the detected optical power (0.1–1 mW), which is typical for laser ultrasonic detection, this problem can also be solved by using small-size detectors with only one pair of surface electrodes. As compared with the AIDC's devices, this photodetector configuration obviously possesses advantages of much more simple design and of more efficient utilization of the incident light power. The inter-electrode distance in these devices is to be of several optimal fringe spacings ($\Lambda_{opt} = 2\pi L_D$, where L_D is the effective mobile photocarrier diffusion length) only. High concentration of the impinging light energy results, however, in significant reduction of the dielectric relaxation time and hence in an excessive growth of the cut-off frequency of the monopolar photo-EMF detector. For the typical detected optical powers mentioned above, the cut-off frequency will be shifted above the frequency band of interest (i.e. 1–30 MHz, where the detected ultrasonic signals are located), which, in its turn, will result in reduced effective sensitivity of the device.

This is, however, not an issue for the bipolar photoconductors where the cut-off frequency of the photo-EMF response is determined by the life-time of slow photocarriers and, as a result, is the light intensity independent [5]. Potentially, the bipolar photoconductive crystals appear to be optimal for such small "one-pair electrode" photo-EMF detectors for laser ultrasonic applications. As a result, search for new bipolar photoconductors suitable for effective utilization in the mentioned above wavelength ranges is of major importance for development of high performance photo-EMF detectors.

Recently in [13] we reported preliminary results on observation of the photo-EMF effect in CdTe:V crystal, governed by essentially bipolar photoconductivity. Unlike GaAs which has smaller bandgap energy, the fundamental absorption edge of CdTe locates at ≈821 nm, which proves to be in close proximity to the spectral region covered by commercially available semiconductor GaAlAs lasers (820–850 nm). The abundant availability of laser wavelengths in this spectral region allows us to match the properties of the CdTe:V photo-EMF detectors to specific requirements of individual applications. Note that for the mentioned above spectral region, the CdTe crystals demonstrate impurity photoconductivity with different photogeneration rates for electrons and holes. As a result, unlike GaAs with interband optical transitions observed for these wavelengths, the CdTe:V photo-EMF detectors are characterized by larger acceptance angle [12]. Furthermore, the CdTe:V crystals offer the flexibility of growing them either with monopolar or with bipolar photoconductivity (both of n- and of p-type—see also [14,15]).

In this paper we present results of a detailed investigation of the photo-EMF effect in bipolar CdTe:V crystals in near IR spectral region ≈826–853 nm close to the fundamental edge of the crystal optical absorption. Together with the data on conventional photoconductivity in this crystal, the presented results enable optimization of the CdTe:V photo-EMF detectors. To the best of our knowledge, no results on the wavelength dependence of the photo-EMF effect in a spectral region close to the fundamental absorption were reported for this or for any other semiconductor earlier. Note also that CdTe:V demonstrates excellent photorefractive properties in the near IR spectral region ≈1–1.5 μm [14–16] and the results presented below can be useful for better understanding and optimization of their photorefractive properties as well.

2. Experimental setup and results

The experimental setup used in this work for characterization of the photo-EMF response is a conventional one—see Fig. 2. As a source of coherent radiation in the spectral region of 826–853 nm we used a tunable external cavity semiconductor EOSI 2010 M laser with diode module DMD 830-015 which ensures linearly polarized cw 10 mW output power. Positive lens and two anamorphic prisms were used to illuminate the input plane of the crystal by two crossing beams with elliptic cross-section of $\approx 1.9 \times 3.8$ mm^2 and without any significant angular divergence. CONOPTICS-380 electro-optic light modulator was used to introduce phase modulation in one of the beams forming the interference pattern.

In the following experiments we used the vanadium doped CdTe crystal of a cubic symmetry (which are usually used in photorefractive experiments [14–16]) which was grown at Brimrose Corporation of America. Two parallel stripe Au electrodes were evaporated on the front (1 1 1)-oriented sample surface with an inter-electrode distance

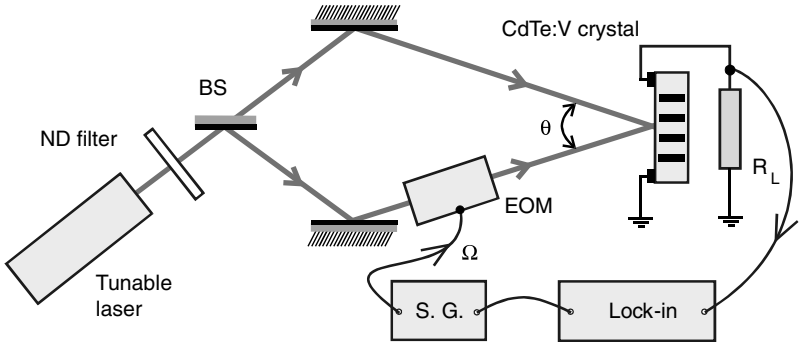

Fig. 2. Experimental configuration used for characterization of the photo-EMF response in CdTe:V crystal.

of $L_x \approx 1.5$ mm. Taking into account the crystal cubic symmetry, no special attention was paid to orientation of the electrodes to the crystallographic axes. The sample was short-circuited through a load resistor R_L (10 or 1 kΩ) and connected by a 50 Ω cable (of ≈30 cm length) to the input of high-frequency lock-in amplifier SRS-844. In case of detection of ultrasonic signals, the CdTe:V sample was connected directly to the input terminals of the Analog Modules transimpedance amplifier 312A-3-1PP (with ≈1 pA/Hz$^{1/2}$ of the input noise current and with 10^6 V/A gain in the 30 MHz frequency band [4]) in order to reduce the input circuit capacitance. The output signal from the amplifier was observed and evaluated using a digital oscilloscope.

Fig. 3 shows the optical transmission of the 1.1 mm thick CdTe:V sample measured in the spectral region of our laser source. Fig. 3 also presents results on conventional photoconductivity of the sample measured under application of an external dc bias voltage U_0. These measurements were performed using periodic modulation of the spatially uniform illuminating light power using the same electro-optic modulator operated in the intensity modulation mode with an additional output polarizer. The spectral profile of the photoconductivity has a well pronounced maximum located at $\lambda_{cond} \approx 835$ nm.

Note that similar behavior of the photoconductivity in the spectral region close to the fundamental absorption edge of the material was also reported in [14] for the CdTe:V samples with different types of dominating photoconductivity. The photoconductivity reduction observed at shorter wavelength side of the peak was also explained in [14] by growing influence of the photocarrier surface recombination [17] at low penetration depth of the light. In our experimental configuration, the reduced detected photocurrent observed at longer wavelengths (with deeper light penetration into the sample) can be partially attributed to the shadowed crystal areas behind the surface electrodes. Another, more fundamental, reason of this decay can be reduction in quantum efficiency of photoconductivity [9] observed for larger wavelengths. By this we mean possible growth of a relative contribution of the other type of centers (not photoconductivity-active) into the total

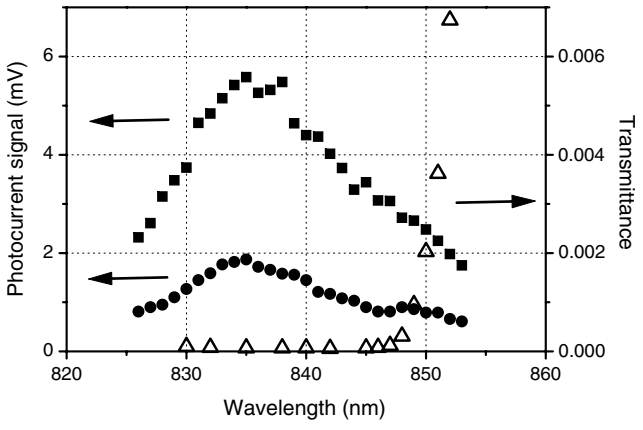

Fig. 3. Wavelength dependences of the conventional photocurrent observed under application of external bias voltage $U_0 = 9$ V at different modulation frequencies $\Omega/2\pi$, kHz: (■) 2, (●) 70 ($R_L = 10$ kΩ) and of the optical transmittance measured for ≈1.1 mm thick sample (△).

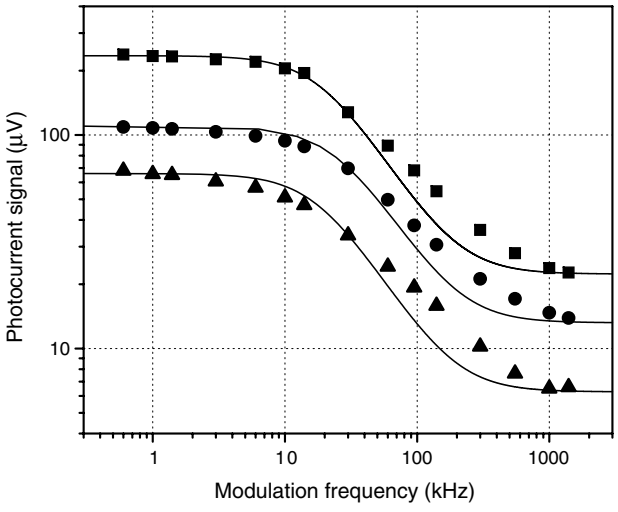

Fig. 4. Modulation frequency dependences of conventional photocurrent measured at different wavelengths λ, nm: (●) 826, (■) 835, (▲) 850 ($U_0 = 9$ V, $R_L = 1$ kΩ, data are corrected for transfer function of the input circuit). Solid lines show the theoretical dependence of the photocurrent (Eq. (1)) absolute value, where $\sigma_f/\sigma_0 = 0.12$, 0.095, and 0.095 and $\tau = 6.5$, 8.5, and 9 μs were used as fitting parameters for the experimental data obtained at the wavelengths 826, 835 and 850 nm, respectively.

light absorption, that can be observed as a result of reduction in absorption by photoconductivity-active centers.

Fig. 4 depicts the modulation frequency dependence of the photoconductivity observed at different wavelengths. In order to reduce the RC product of the input circuit, the load resistance was chosen to be rather low ($R_L = 1$ kΩ) in these measurements. The photocurrent data were additionally corrected for the cut-off frequency of the detection circuit (≈1.5 MHz). As one can see from Fig. 4 the detected photocurrents proved to be frequency independent up to some characteristic cut-off frequency Ω_{ph}. The first plateau was followed by some decay and then the signal reached another plateau. For typical conditions of our measurements the photoconductivity signal was linear on the external dc bias and a little bit sublinear on the average illuminating light power, as shown in Fig. 5.

We also measured a variety of photo-EMF characteristics in the same spectral region. Note that since the photo-EMF signals are significantly lower than conventional photocurrents, the minimal value of the load resistor which we could use in this case was 10 kΩ, which limited the frequency range of our photo-EMF measurements by 100 kHz. Fig. 6 presents the photo-EMF signal dependence on the modulation frequency Ω. The shape of this dependence is quite typical [1]: after a certain characteristic cut-off frequency Ω_0, the initial, approximately linear growth is changed by a plateau (some insignificant decay at high frequency end can be attributed to $R_L C \approx 0.6$ μs of the amplifier input circuit). Note that the value of Ω_0 did not depend on the average incident light intensity and corresponded well to the cut-off frequency observed in the photoconductivity curve (Fig. 4). As the conventional photocurrent (Fig. 5b), the detected photo-EMF signal also demonstrated a little bit sublinear dependence on the average light intensity both below and above the cut-off frequency.

Fig. 7 presents the beam crossing angle θ dependence of the photo-EMF signal amplitude measured at different wavelengths and for modulation frequency significantly higher than the above-mentioned cut-off frequency. The curves exhibit quite typical shape of the photo-EMF response [1]: after reaching a maximum the initial linear growth of the photo-EMF current changes for a relatively slow ($\propto\theta^{-1}$) decay. One can also see that the position of maxima in these curves is wavelength dependent.

Fig. 8 shows the wavelength dependence of the photo-EMF signal amplitude measured for high modulation frequencies (i.e. higher than the cut-off frequency Ω_0) and for small crossing angle $\theta = 0.007$ rad., i.e. below the crossing angles for which the maximal output signals are reached. One can see that like conventional photoconductivity, there is also a quite pronounced maximum here.

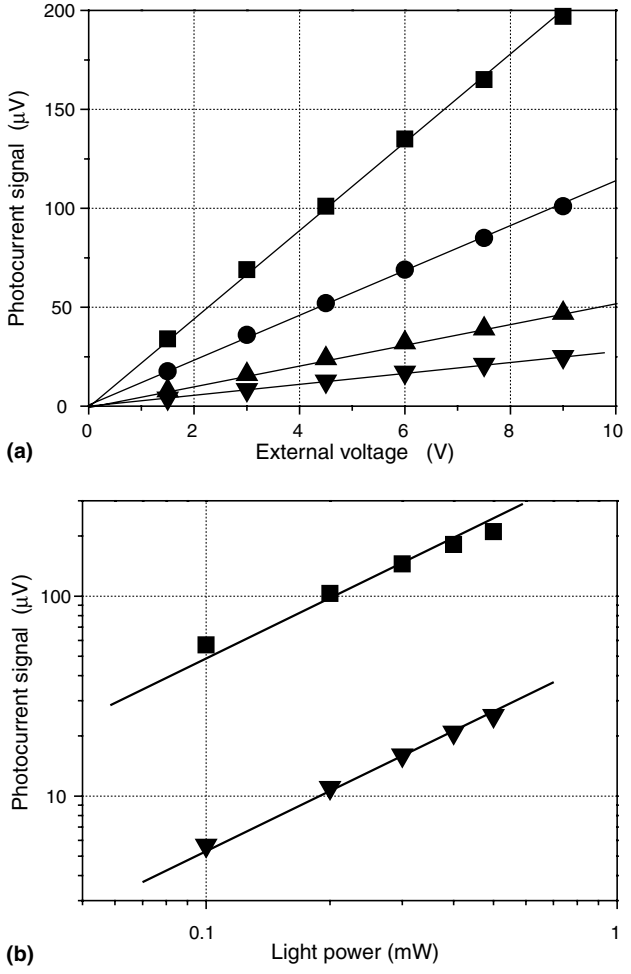

Fig. 5. Dc voltage (a) and average intensity (b) dependences of conventional photocurrent observed at $\lambda = 830$ nm and different modulation frequencies $\Omega/2\pi$, kHz: (■) 30, (●) 95, (▲) 300, (▼) 1000 ($R_L = 1$ kΩ, rectangular amplitude modulation). The curves (a) were obtained at maximal incident power and the curves (b) for external voltage 9 V. The solid lines show linear approximations.

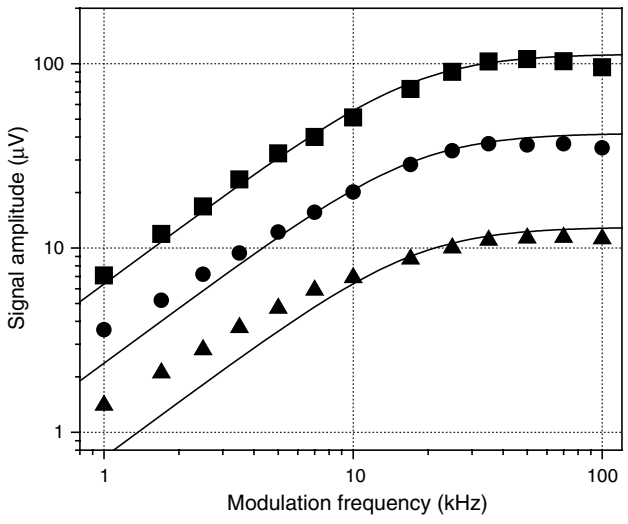

Fig. 6. Modulation frequency dependence of the photo-EMF signal measured with $R_L = 10$ kΩ at wavelength of maximal response $\lambda = 840$ nm and at spatial frequency $K = 53$ mm^{-1} (beam crossing angle $\theta \approx 0.007$) for different average intensities I_0; mW/cm^2: (■) 64, (●) 16 and (▲) 3.2. The solid lines represent theoretical curves calculated for the characteristic time = 9 μs used as a fitting parameter for all three curves.

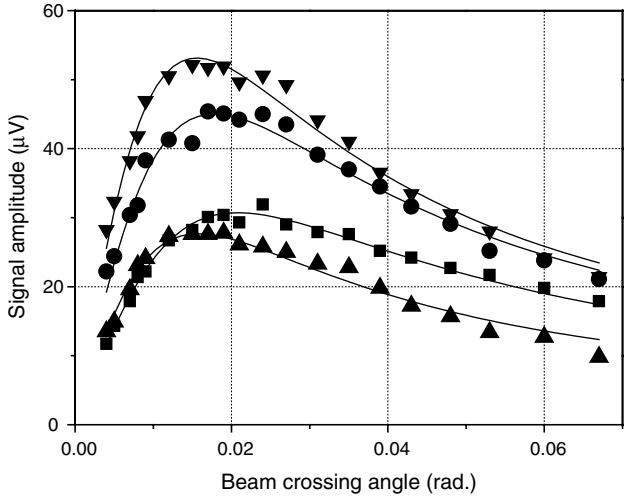

Fig. 7. Beam crossing angle dependence of the photo-EMF signal measured at modulation frequency $\Omega/2\pi = 50$ kHz for different wavelengths λ, nm: (■) 830, (●) 835, (▼) 840, and (▲) 850 ($I_0 = 16$ mW/cm^2, $\Delta = 0.3$ rad, $R_L = 10$ kΩ). The solid lines show theoretical approximations, where the maximal photo-EMF signal and the carrier diffusion length evaluated from Fig. 8 were used as fitting parameters.

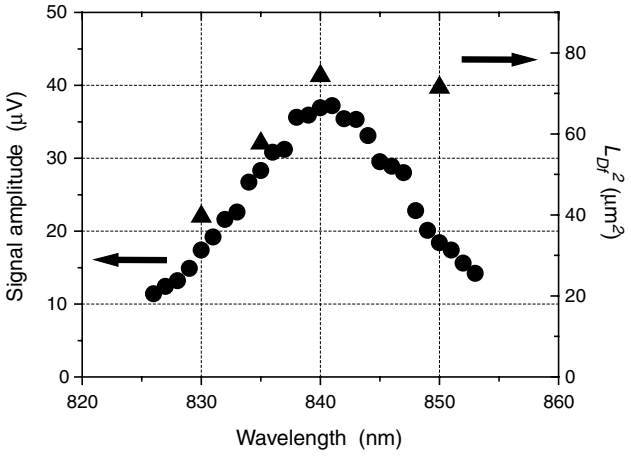

Fig. 8. Spectral dependence of the photo-EMF response measured at high modulation frequency $\Omega/2\pi = 50$ kHz ($I_0 = 16$ mW/cm^2, $\theta \approx 0.007$, $\Delta = 0.3$ rad, $R_L = 10$ kΩ)—(●). Triangles show the squared photocarrier diffusion length L_D^2 used in fitting the experimental curves presented in Fig. 7.

Its position proved to be shifted from the corresponding maximum of the photoconductivity to the wavelength ≈840 nm.

3. Discussion

Utilization of the light wavelength below fundamental absorption edge of the material implies impurity photoconductivity of a monopolar or bipolar type. The modulation frequency dependence of the photoconductivity presented in Fig. 4 allows us to assume that we have the latter case in the experiments reported here. Indeed, if we assume that one type of the photocarriers (which we address below as "slow") has relatively long lifetime τ while the other photocarrier type ("fast") has negligibly short lifetime as compared with the typical period of modulation used in the experiments, the corresponding theoretical equation for the photocurrent can be written in the following form:

$$J_{ph}(\Omega) \propto U_0\sigma_0 \frac{1 + i\Omega\tau(\sigma_f/\sigma_0)}{1 + i\Omega\tau} \quad (1)$$

Here U_0 is the externally applied dc voltage, $\sigma_0 = \sigma_f + \sigma_s$ is the total photoconductivity, and $\sigma_{f,s}$ are the photoconductivity components corresponding to fast and to slow carriers, respectively. The above equation was obtained as a result of consideration of conventional photocarrier rate equations with sinusoidal modulation of a spatially uniform light intensity. In calculation of the total current we have also neglected the displacement component, which is justified when the dielectric relaxation time of the illuminated sample is shorter than the inverse modulation frequency ($\tau_{di} \ll \Omega^{-1}$). There are two plateaus in the predicted photoconductivity response, and the ratio between the photocurrents measured at high and at low modulation frequencies determines the relative contribution of fast photocarriers to the total conductivity σ_f/σ_0.

The theoretical curves corresponding to the experimental data are shown in Fig. 4 by solid lines. For fitting the dependences observed at $\lambda = 850$, 835 and 826 nm we used $\sigma_f/\sigma_0 = 0.095$, 0.095, 0.12 and $\tau = 9$, 8.5, 6.5 μs, respectively. In the fitting procedure we were interested first of all in the better matching of the beginning of the decaying parts of the curves, which have significantly larger amplitude. From Fig. 4 one can see that the theory does not describe the experiment perfectly well: all the experimental dependences demonstrate slower decay with modulation frequency. It is probable that slow photocarriers cannot be characterized by one relaxation time only, which corresponds to the assumption used in derivation of Eq. (1).

It can be seen, however, from Fig. 4 that the slow photocarriers are dominant in the CdTe:V crystal under investigation, the admixture of the minority photoconductivity is typically about 10–13%. Note that fitting of the data obtained at shorter wavelength needed smaller characteristic times, which agrees with a general reduction of the photoconductivity towards this end of the investigated spectral region. The minority photocarriers have an effective life-time shorter than we could measure using the modulation frequencies ≈1.4 MHz allowed by our experimental set up, i.e. it is smaller than ≈0.1 μs.

In general, depending on the ratio between the photocarrier life-time τ and the dielectric relaxation time τ_{di}, the photo-EMF effect under consideration can be classified into two main categories [1]. In one case (see also [18]), when $\tau_{di} \gg \tau$, the dynamics of the photo-EMF signal formation is governed by the dielectric relaxation in the illuminated sample and in the other case, when $\tau_{di} \ll \tau$, it is governed by the life-time of photocarriers (as, for example, in semiinsulating GaAs in visible/near IR spectral region [5]). In the former case the cut-off frequency of the

photo-EMF signal $\Omega_0 \approx \tau_{di}^{-1}$ grows linearly with the average light intensity, and the signal amplitude observed at modulation frequency $\Omega \leqslant \Omega_0$ proves to be intensity independent. On the opposite, in the latter case the cut-off frequency $\Omega_0 \approx \tau^{-1}$ is intensity independent and the photo-EMF signal amplitude grows linearly with the light intensity at modulation frequencies both below and above the cut-off frequency.

As it was mentioned above, the cut-off frequency of the photo-EMF effect observed in the investigated CdTe:V is light intensity independent (see Fig. 6) and its value approximately corresponds to the cut-off frequency of the photoconductivity response (Fig. 4) $\Omega_0 \approx \tau^{-1}$. This clearly leads to the conclusion that dynamics of the observed photo-EMF effect is determined by the life-time of slow photocarriers, which in this case should also be significantly larger than the dielectric relaxation time of the illuminated crystal. In general this conclusion seems to be reasonable: due to strong light absorption the photoconductivity of the CdTe:V sample is quite high and the dielectric relaxation time in the near-surface layer of the sample where the photo-EMF signal is effectively formed can be quite short in the investigated spectral region (see also [9]).

In case when the photo-EMF signal is formed predominantly by one type of photocarriers with $\tau \gg \tau_{di}$, one can show [1,19] that the maximal photo-EMF current is approximately $\chi \approx \tau_{di}/\tau$ times smaller than in the material with the same average photoconductivity but with $\tau \ll \tau_{di}$. In this case addition of minority photocarriers of the opposite sign with similar life-time can only reduce the photo-EMF signal because of electron–hole competition in formation of the space charge grating (note that this is also correct when $\tau \gg \tau_{di}$). However, some admixture of fast minority photocarriers (i.e. with the life-time significantly shorter than τ_{di}) can increase the amplitude of the photo-EMF current generated at $\Omega < \tau_{di}^{-1}$ dramatically. Simplifying, one can say that in this case, the slow dominating carriers produce a stable pattern of the space charge field grating mainly, while the output signal is generated by the vibrating pattern of photoconductivity associated with fast photocarriers. The cut-off frequency of the photo-EMF response is fixed and equal to the inverse of the life-time of the slow photocarriers; and the amplitude of the signal grows proportionally with the average light intensity both below and above the cut-off frequency. As it was mentioned above in the experimental section, both of these features were observed in our CdTe:V sample.

In addition to the reasonable qualitative behavior, quantitative agreement of the experimentally observed amplitude of the photo-EMF signal with its theoretical evaluation is also very important. Below we use the following theoretical equation for the density of the short-circuit photo-EMF current, which was obtained in [1,5] in conventional approximation of low amplitude of the phase modulation ($\Delta \ll 1$) and of the interference pattern contrast ($m \ll 1$) for an intermediate region of the modulation frequencies $\tau^{-1} \ll \Omega \ll \tau_{di}^{-1}$:

$$j^{\Omega} = -\frac{\Delta m^2}{2} E_D \sigma_0 \frac{2\sigma_f \sigma_s}{\sigma_0^2} \times \frac{1 + K^2\left(\frac{\sigma_s}{\sigma_0} L_{Df}^2 - \frac{\sigma_f}{\sigma_0} L_{Ds}^2\right)}{\left(1 + K^2 \frac{\sigma_s}{\sigma_0} L_{Df}^2\right)\left[1 + K^2\left(\frac{\sigma_s}{\sigma_0} L_{Df}^2 + \frac{\sigma_f}{\sigma_0} L_{Ds}^2\right)\right]} \quad (2)$$

Here $E_D = Kk_BT/e$ is the diffusion field, K is the grating spatial frequency, and $L_{Df,s}$ are the diffusion lengths of fast and slow photocarriers, respectively. Additionally it was assumed that the fast carrier life-time is shorter than the dielectric relaxation time τ_{di}. Note that the sign of the photocurrent presented above corresponds to the assumption made in [1,5] that the slow carriers are holes.

With additional assumption $(\sigma_s/\sigma_0)L_{Df}^2 \gg (\sigma_f/\sigma_0)L_{Ds}^2$ (which means much larger generation rate of slow photocarriers) the above equation reduces to:

$$j^{\Omega} = -\frac{\Delta m^2}{2} E_D \sigma_0 \frac{2\sigma_f \sigma_s}{\sigma_0^2} \frac{1}{1 + K^2 \frac{\sigma_s}{\sigma_0} L_{Df}^2} \quad (3)$$

This equation predicts, in particular, that spatial frequency dependence of the photo-EMF signal has quite conventional form: the initial linear growth with K ($E_D \propto K$) is followed by maximum at $K = [(\sigma_s/\sigma_0)L_{Df}^2]^{-1/2}$ and, after this, by inverse linear decay $\propto K^{-1}$. Note that for equal generation rates of the photocarriers observed, in particular, in GaAs for interband optical excitation [5], the decay is much faster ($\propto K^{-3}$), and for larger generation rate of the fast photocarriers Eq. (2) predicts change of the signal sign with growing K. Following simplification of Eq. (3) in approximation of a short diffusion length of the photocarriers $(\sigma_s/\sigma_0)K^2L_{Df}^2 \ll 1$ results in:

$$j^{\Omega} = -\frac{\Delta m^2}{2} E_D \sigma_0 \frac{2\sigma_f \sigma_s}{\sigma_0^2} \quad (4)$$

From here one can see that the maximal photo-EMF response observed is by factor $2\sigma_f\sigma_s/\sigma_0^2$ smaller than that [1,18] in the monopolar photoconductor of the same photoconductivity σ_0 and with $\tau \ll \tau_{di}$.

The quantitative evaluation of the observed photo-EMF signal amplitude is usually made using the fundamental relation for a maximal amplitude of the photo-EMF response observed in the mentioned above monopolar photoconductor at modulation frequency $\Omega \gg \tau_{di}^{-1}$ and at low spatial frequency $K \ll L_D^{-1}$. In this case, the amplitude of the photo-EMF current is given by [1,18]:

$$|J^{\Omega}| = \frac{\Delta m^2 E_D}{2} \frac{J_{pc}}{E_0} \quad (5)$$

where J_{pc} is the conventional dc photocurrent measured in the same sample under similar spatially uniform illumination in externally applied field E_0. For CdTe:V sample discussed here, the theoretical evaluation based on Eq. (5) and on direct additional measurement of the dc photocurrent J_{pc} led to the value of J^{Ω} that is approximately ≈3–4 times larger than that observed experimentally. This corresponds reasonably well to the additional loss factor $2\sigma_s\sigma_f/\sigma_0^2$ (see

Eq. (4)) calculated for the experimentally observed (see Fig. 4) value $\sigma_f/\sigma_0 \approx 0.1$.

As it was mentioned above, in the accepted model of the photo-EMF signal formation the position of maximum in the crossing angle dependence (see Fig. 7) is governed by the diffusion spreading of fast photocarriers (see Eq. (3)). In case under consideration when $\sigma_f/\sigma_0 \ll 1$ (see Fig. 4) the spatial frequency corresponding to this maximum approximately equals the inverse diffusion length of these photocarriers, i.e. $K_{opt} \approx L_{Df}^{-1}$. As evaluated from Fig. 7, the photocarrier diffusion length $L_{Df} = \sqrt{D_f \tau_f}$ (where D_f is the corresponding photocarrier diffusion coefficient) drops from its maximal value about 8.5 μm observed in 840–850 nm spectral region the diminishing wavelength up to approximately 6.3 μm at 830 nm—see Fig. 8.

Note also that, at least for the short wavelengths, similar behavior of the photo-EMF signal amplitude and of L_{Df}^2 (Fig. 8) is quite natural and supports the accepted model of the photo-EMF signal formation. Indeed, in accordance with Eq. (3) the photo-EMF signal amplitude is proportional to the product $\sigma_0(2\sigma_s\sigma_f/\sigma_0^2)$ which for dominating slow photocarriers ($\sigma_s \gg \sigma_f$) is approximately equal to $2\sigma_f$ i.e. the photo-EMF signal proves to be proportional to the fast photoconductivity component. Taking into account the Einstein relation $D_f/\mu_f = k_B T/e$ (where μ_f is the fast photocarrier mobility) we obtain $J^{\Omega}(\lambda) \propto \sigma_f(\lambda) \propto L_{Df}^2(\lambda)$. Additional decay of the photo-EMF signal amplitude observed at longer wavelengths (Fig. 8) can be attributed, as it was mentioned above, to the shadowing by the electrodes or to the reduced quantum efficiency of photoconductivity. Neither of these two reasons can affect the diffusion length of the fast carriers.

The sign of the generated photo-EMF signal is determined by slow photocarriers, which are responsible for formation of a stable (i.e. not vibrating) space charge grating. We determined the type of these photocarriers by comparing the sign of the photo-EMF signals generated in the sample under investigation with that observed in a monopolar CdTe:V, where in the experiments reported in [9] the dominating photocarriers were identified as electrons. Oscilloscope traces of the detected laser generated ultrasound signals are given in Fig. 9, from which one can see that polarity of the signal detected by bipolar CdTe:V device proved to be the opposite to that generated by the monopolar CdTe:V one. Hence, the fast photoconductivity component in the sample under consideration (as well in a monopolar CdTe:V sample investigated in [9]) is associated with the photoelectrons.

Note that the photoelectrons diffusion length evaluated in the bipolar CdTe:V sample proved to be approximately three times larger than that in the monopolar CdTe:V crystal [9] (≈2.5 μm at 852 nm). On the other hand, it is significantly (i.e. by nearly two orders of magnitude) larger than another characteristic length associated with saturation of trapping centers during the space charge grating formation, namely, the Debye screening length L'_D. Indeed, as it was shown in [14] from the results of investigation of the steady-state two-wave energy exchange at the photorefractive grating, this length is typically around ≈0.1 μm in CdTe:V, no matter which type of the dominating photocarrier it has. As it was shown for monopolar photoconductors [1,20], when $L'_D \geqslant L_D$ the saturation of trapping centers rather than the carrier diffusion governs the shape of the spatial frequency dependence of the photo-EMF amplitude. As far as we know, no theoretical models of the photo-EMF in bipolar photoconductors which also take into account saturation of trapping centers were developed until the present moment. Mentioned above significant discrepancy between the characteristic values of L'_D reported for CdTe:V and the experimentally observed positions of maxima in the crossing angle dependence in Fig. 7 makes this alternative model highly improbable for the CdTe:V sample in question.

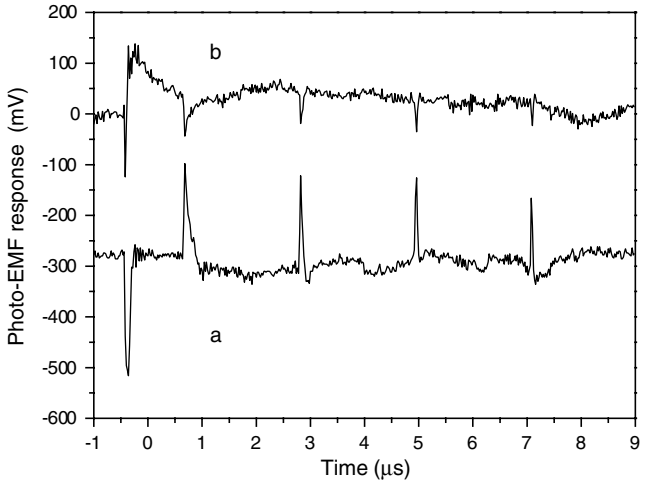

Fig. 9. Typical output signals generated by monopolar (a) and bipolar (b) CdTe:V based photo-EMF detectors in laser-induced ultrasonic detection configuration presented in Fig. 1. Wavelength of the probe beam $\lambda = 852$ nm, crossing angle $\theta = 0.1$ rad, and total power in the inter-electrode spacing ≈1 mW. The ultrasonic wave was generated by the 800 mJ, 10 ns pulsed Nd:YAG laser (at $\lambda = 1.06$ μm).

Let us also note in conclusion that the oscilloscope traces presented in Fig. 9 show clear superiority of the monopolar photo-EMF device over the bipolar one. At least partly it is because the spatial frequency used was far from the optimal one for the bipolar device. The concentration of the detected light power was also not so strong in these experiments. Further reduction of the photodetector size to that of the optimal small-size device will need for significant concentration of the detected light power. As it was mentioned above, this is to be accompanied by reduction of the photodetector cut-off frequency and by reduced responsivity of the monopolar device in the MHz frequency region of interest.

4. Conclusion

We have presented experimental results on the wavelength dependence of basic parameters of the photo-EMF

effect in a CdTe:V crystal. The data were obtained in the spectral region of 826–853 nm, close to the fundamental absorption edge of CdTe, where this material demonstrates photoconductivity of the impurity type. It was shown that the dynamics of the generated photo-EMF signal is governed by the life-time ($\tau \approx 6$–9 μs) of the dominating slow photo-carriers, namely, holes. The main characteristic features of the observed effect (position of the cut-off frequency, its independence on the average light intensity, shape of the crossing angle dependence, and the absolute value of the generated signal) proved to be in a good agreement with the theoretical model of the photo-EMF effect developed for a bipolar impurity photoconductor with life-time of one photocarrier significantly larger than the dielectric relaxation time of the illuminated sample. This can be considered as a demonstration of reliability of the photo-EMF excited by vibrating interference pattern as a simple and flexible technique for characterization of minority photocarriers (in particular, for evaluation of their diffusion length) in semiconductors [21]. The obtained results also show possibility of a significant improvement of the photo-EMF detectors based on bipolar CdTe:V by tailoring the probe laser wavelength in the investigated spectral region, which overlaps with spectral region of commercially available semiconductor GaAlAs lasers.

References

[1] S. Stepanov, Photo-electromotive-force effect in semiconductors, in: H.S. Nalwa (Ed.), Handbook of Advanced Electronic and Photonic Materials and Devices, Vol. 2, Academic Press, San Diego, 2001, p. 205.
[2] R.J. Dewhurst, Q. Shan, Meas. Sci. Technol. 10 (1999) R139.
[3] P.V. Mitchell, G.J. Dunning, S.W. McCahon, M.B. Klein, T.R. O'Meara, D.M. Pepper, Compensated high bandwidth laser ultrasonic detector based on photo-induced EMF in GaAs, in: D.O. Thompson, D.E. Chimenti (Eds.), Review of Progress in Quantitative Evaluation, Vol. 15, Plenum, NY, 1996, p. 2149.
[4] http://www.analogmodules.com/products.htm.
[5] N. Korneev, S. Mansurova, S. Stepanov, T.J. Hall, A.K. Powell, JOSA B 13 (1996) 2278.
[6] C.C. Wang, S. Trivedi, F. Jin, K. Jia, H. He, G. Elliot, J. Khurgin, JOSA B 19 (2002) 177.
[7] C.C. Wang, S. Trivedi, F. Jin, J. Khurgin, D. Temple, U. Hommerich, E. Gad, F.-S. Choa, J. Ligthwave Technol. 19 (2001) 666.
[8] P. Rodríguez, S. Trivedi, F. Jin, C.C. Wang, S. Stepanov, G. Elliott, J.F. Mayers, J. Lee, J. Khurgin, Appl. Phys. Lett. 83 (2003) 1893.
[9] S. Stepanov, P. Rodríguez, S. Trivedi, C.C. Wang, Appl. Phys. Lett. 84 (2004) 446.
[10] D.D. Nolte, J.A. Coy, G.J. Dunning, D.M. Pepper, M.P. Chiao, G.D. Bacher, M.B. Klein, Opt. Lett. 24 (1999) 342.
[11] J.A. Coy, D.D. Nolte, G.J. Dunning, D.M. Pepper, B. Pouet, G.D. Bacher, M.B. Klein, JOSA B 17 (2000) 697.
[12] S. Stepanov, P. Rodríguez, S. Trivedi, C.C. Wang, Nondestruct. Test. Eval. 19 (3) (2003) 91.
[13] P. Rodríguez, M.L. Arroyo, S. Mansurova, S. Stepanov, S. Trivedi, C.C. Wang, Wavelength dependence of the photo-electromotive-force effect in bipolar CdTe:V—Tech. Digest of CLEO'04, San-Francisco, USA, May 2004, CMBB7.
[14] L.A. de Montmorillon, Ph. Delaye, G. Roosen, H. Bou Rjeily, F. Ramaz, B. Briat, J.G. Gies, J.P. Zielinger, M. Tapiero, H.J. von Bardeleben, T. Arnoux, J.C. Launay, JOSA B 13 (1996) 2341.
[15] Ph. Delaye, L.A. Montmorillon, I. Biaggio, J.C. Launay, G. Roosen, Opt. Commun. 134 (1997) 580.
[16] J. Millerd, M. Ziari, A. Partovi, Photorefractivity in semiconductors, in: E. Garmire, A. Kost (Eds.), Nonlinear Optics in Semiconductors I, Semiconductors and Semimetals, Vol. 58, Academic Press, London, 1999.
[17] R.H. Bube, Photoelectronic Properties of Semiconductors, Cambridge University Press, Cambridge, 1992.
[18] M.P. Petrov, I.A. Sokolov, S.I. Stepanov, G.S. Trofimov, J. Appl. Phys. 68 (1990) 2216.
[19] I.A. Sokolov, S.I. Stepanov, Electron. Lett. 26 (1990) 1275.
[20] I. Seres, S. Stepanov, S. Mansurova, JOSA B 17 (2000) 1986.
[21] J.W. Orton, P. Blood, The Electrical Characterization of Semiconductors: Measurements of Minority Carrier Properties, Academic Press, London, 1990.